SAND2014-15359C

Analysis of the Equation of State and Initiation Model for TATB-based LX-17

Seth Root and Leah Tuttle

Sandia National Laboratories, Albuquerque, 87125

Abstract. The unreacted equation of state (EOS) for energetic materials is determined using standard shock or shockless compression experimental methods. For the detonation products, the EOS is typically determined from cylinder expansion tests or the sideways plate push test. The difficulty with these experiments is that the metal acceleration is not a one-dimensional problem. The tests also require the use of an initiation model, which requires analysis as well. In this work, we perform a series of plate-impact experiments to examine the initiation model and detonation product EOS of the TATB-based explosive LX-17. The LX-17 samples are backed by various thicknesses of well-characterized metal buffers (Al, Cu, and Ta) and velocity interferometry measures the velocity profiles at a metal/LiF window interface. The experimentally measured velocity profiles are compared to simulations to determine the effectiveness of the models and optimization methods are used to suggest improvements to the models.

Introduction

The equation of state (EOS) of energetic materials is important for understanding performance and safety of an plastic-bonded explosive (PBX). The unreacted EOS for a PBX is determined through shock compression, Hugoniot measurements[1] and shockless compression techniques using Sandia's VELOCE or Z-Machine[2]. Determining the EOS of the detonation products is a more difficult task. Principal methods used to determine the product EOS are cylinder expansion test[3] or the sideways plate push test[4]. These experiments are inherently multi-dimensional problems, which may introduce complications in the analysis. In the 1940s, Goranson performed one-dimensional experiments using a plane-wave generator to initiate an explosive of interest. The explosive was backed by a metal plate of various thickness and the free surface velocity of the metal plate was measured using contact pins. Plotting the free surface velocity versus the metal plate thickness, Goranson was able to examine the reaction zone width and detonation product EOS.

In this work, we use a modified version of the Goranson experiment to test the initiation model and the detonation product EOS for LX-17. LX-17 is a triaminotrinitrobenzene (TATB) based explosive with nominally 7.5% binder by weight. TATB-based explosives are of interest because of their extreme insensitivity to impact. LX-17 has been studied under several conditions and several models exist for the detonation products. We examined potential EOS models for the unreacted and reacted LX-17 as well as the initiation model using CTH simulations and comparing to our experimental results. Optimization methods are used to modify model behavior to match experimental data.

Experimental Approach and Results

For the experiments discussed here, we used LX-17-1 manufactured by Holston Defense Corporation with lot number HOL87M851-010. Analysis of the blend showed an average of 92.5% TATB and 7.5% Kel-F 800 with trace amounts of other volatiles.

All experiments were conducted using the 90mm-bore powder gun at Sandia's STAR facility. The gun is capable of accelerating projectiles up to 2.2 km/s, which is sufficient to initiate an LX17 sample in a short run-distance. A schematic view of the experiment is shown in Fig. 1. All experiments used a copper impactor (12.7 mm in thickness) accelerated to approximately 2 km/s that impacted the LX-17 sample. The metal inerts were aluminum, copper, or tantalum with thicknesses ranging from 1 mm to 4 mm. The Ta was specified as Annealed, ASTM-B-708 RO5200; the Cu was OFHC ASTM F68; the aluminum was as 6061-T6. We used EpoTek 301 epoxy to bond the LX-17/Inert/LiF sample stacks. An aluminum mirror was coated on the LiF bonding surface and the rear surface was anti-reflected coated for 532 nm. A 19-channel velocity interferometry system for any reflector (VISAR) was used to measure the wave profile at the inert-LiF window interface. VISAR was also used to determine the projectile tilt by detecting impact at the LiF windows around the samples. We used 1.2739 for the VISAR correction for LiF[5] - using the VISAR correction factor of 1.280[6] results in velocities approximately 0.5% lower.

Figure 2 shows an image of a target plate used in the Ta experiments DP01 and DP04. The target plate had 4 LX-17 samples per target plate. The LX-17 samples and metal inerts were nominally 30 mm in diameter. In later experiments, we moved to the large diameter target plate shown in Fig. 3. This target plate configuration was used for the two experiments using copper and aluminum as the metal inerts. The LX-17 sample is 70 mm in diameter instead of 4 $\times$ 30 mm individual samples. The larger diameter sample allowed for VISAR windows to be placed on the LX-17 to measure the detonation profile directly. Time of arrival of the detonation profile was also used to correct for sample tilt within the target plate. Table 1 details the four experimental configurations.

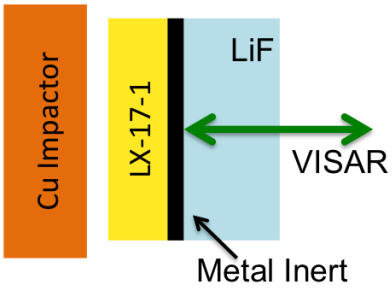

Fig. 1. Schematic view of the experimental configuration

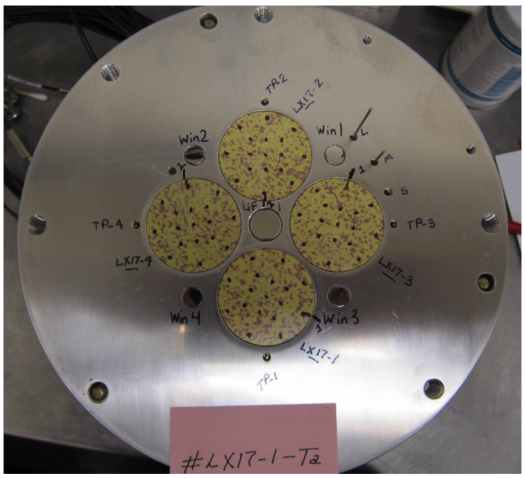

Fig. 2. Image of a completed target used for the Ta experiments with individual target samples.

Table 1. Experimental configuations

Shot ID	V_F (km/s)	LX17 (mm)	Density (g/cc)	Inert (mm)	Imp. Stress (GPa)	Run-to-Det. (mm)
DP01-1-Ta	2.006±0.004	7.988±0.002	1.899	1.017±0.007	16.40	4.15
DP01-2-Ta		8.015±0.002	1.903	2.004±0.005		
DP01-3-Ta		7.987±0.001	1.902	2.978±0.005		
DP01-4-Ta		8.019±0.004	1.904	4.002±0.003		
DP04-1-Ta	1.892±0.004	7.995±0.003	1.903	1.022±0.006	15.13	5.38
DP04-2-Ta		8.002±0.002	1.901	1.977±0.014		
DP04-3-Ta		8.005±0.002	1.902	3.016±0.011		
DP04-4-Ta		7.989±0.002	1.904	3.990±0.005		
DP10-1-Al	2.072±0.006	6.585±0.002	1.894	1.003±0.005	17.09	3.63
DP10-2-Al		6.585±0.002		1.995±0.002		
DP10-3-Al		6.583±0.002		2.989±0.004		
DP11-1-Cu	2.070±0.006	6.589±0.005	1.892	1.009±0.004	17.05	3.66
DP11-2-Cu		6.583±0.003		2.014±0.004		
DP11-3-Cu		6.585±0.003		3.013±0.004		

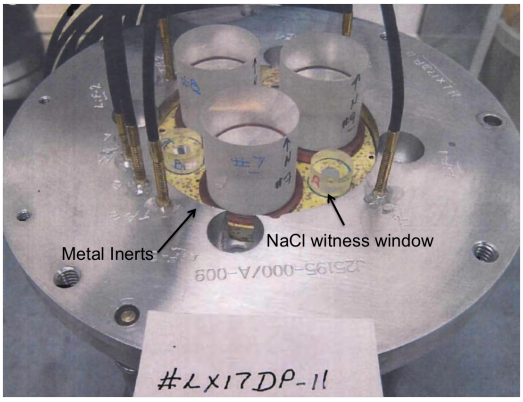

Fig. 3. Image of a completed large diameter sample target used for the Al and Cu experiments.

Experimental Results

The measured wave profiles from the 4 experiments are shown in Figures 4-7. The initial stress in the explosive was calculated using the quadratic Eqn 1 determined from shockless compression experiments.[7] The run distance to detonation was determined using the Pop-Plot fit to LX-17 ($\rho_0 = 1.90$)[8] and is shown in Eqn 2.

$$U_S(km/s) = 2.411 + 2.177U_P - \frac{0.406}{2.411}U_P^2 \quad (1)$$

$$log(x) = (4.53 \pm 0.12) - (3.22 \pm 0.10)log(P) \quad (2)$$

Figure 4 shows the measured velocity profiles from experiment DP01. Looking at the wave profile from the with the 1 mm Ta sample, we see the Talyor wave response expected in a detonation wave. As the inert buffer thickness increases, we see attenuation of the peak velocity at the inert/LiF interface. In the 1 mm and 2 mm inert buffer profiles, a second shock is observed due to the impedance mismatches with the Ta inert. The velocity profiles from DP04, shown in Figure 5 show similar behavior as the DP01 velocity profiles. The timing is shifted between the two experiments because of the differing flyer velocity, which results in a different shock velocity in the unreacted portion of the

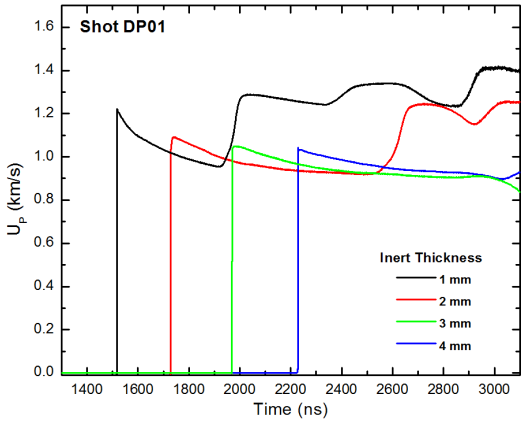

Fig. 4. Measured velocity profiles from experiment DP01.

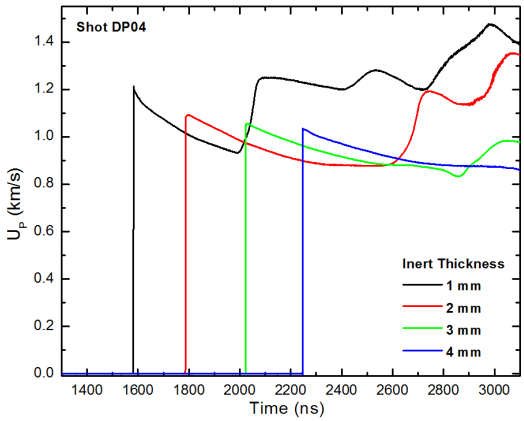

Fig. 5. Measured velocity profiles from experiment DP04 using Ta inerts.

explosive and a different transition to detonation location.

Figure 6 shows the velocity measurements from the experiment using aluminum inert buffer plates. This experiment utilized the larger diameter explosive sample so that the detonation profile could be measured directly the the explosive interface. The profiles from the three LX-17/NaCl interface measurements are also shown in the figure. The three detonation profiles show the expected velocity behavior for a detonation, indicating that detonation did occur within the sample. The three profiles also provide an indication of our timing uncertainty caused by projectile tilt, sample offset in the target plate, etc. For this experiment, the timing uncertainty based on the NaCl detonation profiles is approximately 10 ns, which could correspond to 20 μm of tilt and offset uncertainty. The velocity profiles at the Aluminum/LiF interface again show Taylor wave shape indicating detonation within the LX-17. As the aluminum inert increases in thickness, we see attenuation of the peak velocity at the interface. We do not observe the second shock that was observed in the Ta samples because of the lower impedance of the aluminum inert buffers.

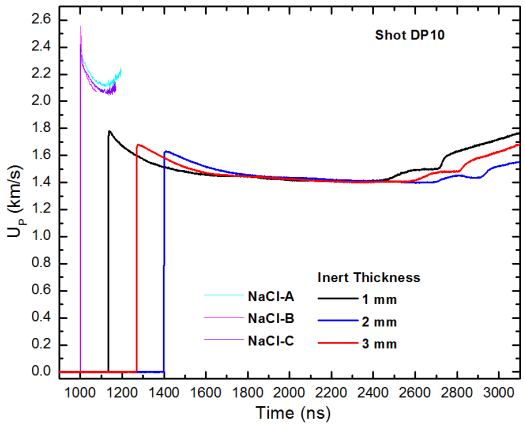

Fig. 6. Measured velocity profiles from experiment DP10 using Al inerts.

Figure 7 shows the measured velocity profiles from the experiment using Cu inerts along with the measurement of the denotation profile at the LX-17/NaCl window interface. We see relatively good agreement in time between the NaCl windows. When compared to the NaCl window measurements in Fig 6, the NaCl-B and NaCl-C measurements match well in time. NaCl-A lies $\approx$ 10 ns outside and may be an indication of some internal porosity or warping in the target. The velocity profiles at the Cu/LiF interface show the Taylor wave decay and a decrease in peak velocity as the sample thickness increases. The sharp spike at the top of the peak is likely caused by the VISAR detector and in the fringe addition and is not a real effect. With the higher impedance of the Cu buffers, we again see the second shock in the profiles later in time. Further experiments using thinner inerts could provide an alternative measure of the reaction zone and using multiple thicknesses of LX-17 would further test the unreacted - initiation model - reacted products

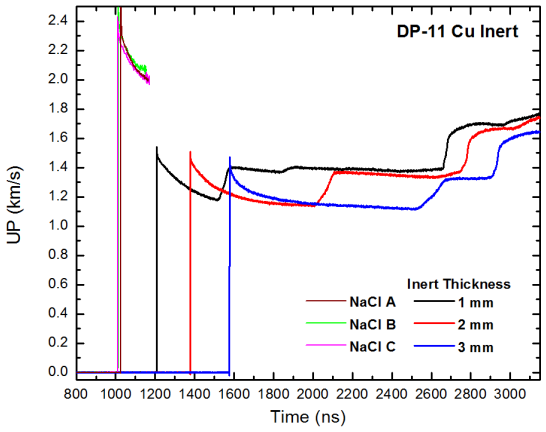

Fig. 7. Measured velocity profiles from experiment DP11 using Cu inerts.

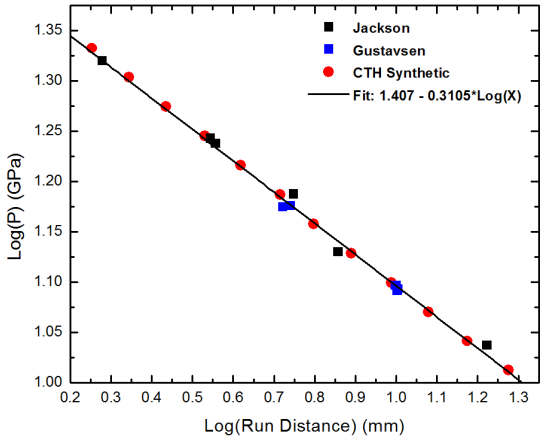

Fig. 8. The synthetic data produced in the HVRB model optimization compared to the experimental Pop-Plot data and corresponding fit.

models.

Simulations

Simulations were performed using Sandia's CTH shock physics code.[9] The simulations requires three components: the unreacted EOS model, the initiation model, and the detonation product EOS model. For the unreacted EOS model we use the quadratic Mie-Gruneisen listed in Eqn 1. The initiation model we use is the History Reactive Variable Burn (HVRB).[10] For the detonation product EOS, we use SESAME Table 9876 that was recently constructed by Hobbs[11] using the JCZS database[12] for LX-17. The EOS used for the inert materials (impactor, inert buffers Al, Cu, and Ta, and the LiF window) were all Mie-Gruneisen with the parameters listed in Table 2. We also implemented a Steinburg-Guinan strength model for the materials using the parameters listed by Steinberg.[13]

Prior to performing the CTH simulations of the experiments, we needed to optimize the HVRB parameters to ensure consistency with the Pop-Plot data from Jackson[14] and Gustavsen.[8] The data from Jackson and Gustavsen were used because of the similarity in initial densities. For the HVRB optimization, we run a series of 1D simulations to generate synthetic Pop-plot data. The sum of the squares of differences between the experimental fit to the Pop-plot data and the synthetic data is minimized by varying two of the HVRB parameters. We optimize the HVRB parameters using the quadratic M-G for the unreacted LX-17 and the SESAME 9876 table and the results are compared to the experimental data in Figure 8.

Figure 9 shows the results from the CTH simulations using the 2-parameter optimization of the HVRB model for the copper inert experiment. Timing of the simulations is early by approximately 40 ns in each thickness, which is outside of the estimated time uncertainty of the experiment. The initial peak velocity is good for the 1 mm inert, but tends to be lower for thicker pieces of copper. The long term velocities were all lower than experimental measured. The results were similar for the simulations using the aluminum inerts shown in Fig 10. Timing was early by approximately 40 ns and late time velocities were all lower. However, the peak velocity was higher than the experimental value. The comparison to the Ta inerts (Figure 11 showed better agreement with the velocity at early times, but in all Ta simulations, the wave arrival was early in the CTH simulations by 70-100 ns. Late time velocities are also lower than experimentally measured. We note that using a different unreacted EOS, such as the linear relation $U_S = 2.33 + 2.32U_P$ from the LLNL Handbook[15] had only a few ns difference in wave arrival.

Optimization of all five parameters in the HVRB model resulted in simulations that could match experiment in time. The wave profiles were up to 5% higher in velocity at the peak, but with lower

Table 2. Mie-Gruneisen parameters used for in the CTH simulations

Material	Density (g/cm^3)	C0 (km/s)	S1	Γ
Al	2.703	5.22	1.37	1.97
Cu	8.93	3.94	1.489	1.99
Ta	16.654	3.39	1.22	1.60
LiF	2.638	5.15	1.35	1.69

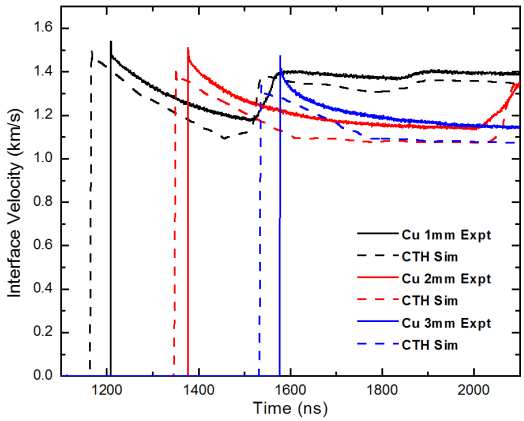

Fig. 9. Comparison of the CTH simulation results using the optimized HVRB parameters and the Hobbs SESAME table for the detonation products for experiment DP11 with copper inerts

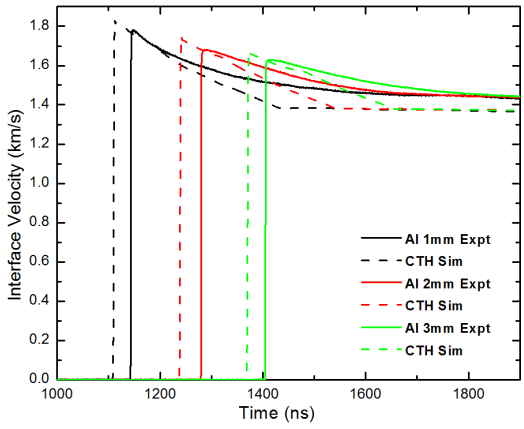

Fig. 10. Comparison of the CTH simulation results using the optimized HVRB parameters and the Hobbs SESAME table for the detonation products for experiment DP10 with aluminum inerts

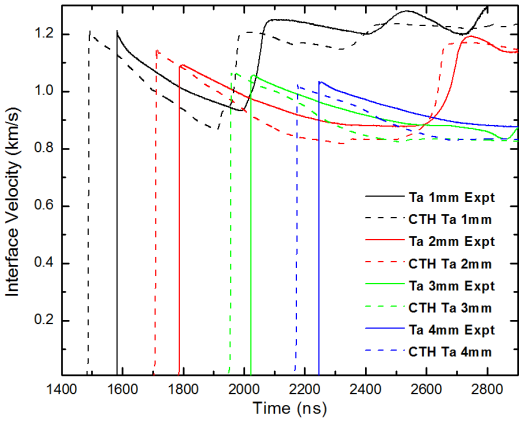

Fig. 11. Comparison of the CTH simulation results using the optimized HVRB parameters and the Hobbs SESAME table for the detonation products for experiment DP04 with tantalum inerts

in velocity at long times when compared to experiment. Figure 12 shows the simulation results using the newly optimized parameters for the HVRB model and their comparison to experiment. The HVRB parameters are the average values of the parameters from the optimization runs on the various thicknesses of the metal inerts. We focused on copper as we expect strength effects to be minimal for copper. As a consequence of the optimization, the new HVRB parameters pushed the synthetic Pop-Plot data to being less sensitive than shown in Figure 8. This suggests that the HVRB model may have difficulties in modeling highly non-ideal explosives or that the detonation product EOS needs refinement and requires comparison to over-driven shock Hugoniot measurements on LX-17. We also tested the JWL EOS and the Ignition and Growth model by Tarver[16], however, the results showed further analysis using these models was needed because of the large number of parameters.[17]

Summary

We have conducted a series of modified-Goranson experiments to examine the equation of state, both unreacted and reacted of LX-17. The experiments are purely 1-D, which may eliminate some of complexities inherent in the cylinder and sandwich plate tests, however, the analysis does require knowledge of the Pop-Plot data. The exper-

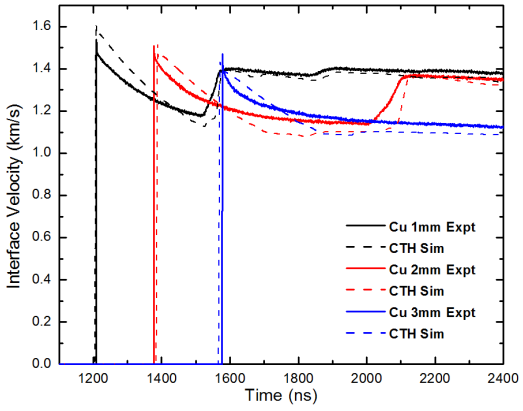

Fig. 12. Simulation results for the copper inert experiment using the average value of the 5 optimized parameters for the three thicknesses of copper. The new values show considerable improvement in time, but inaccuracies in the overall velocity profiles.

imental results were compared to CTH simulation data to examine the EOS and the initiation model. The initiation model was optimized to experimental Pop-Plot data using a M-G unreacted EOS and a recently developed SESAME table for the reaction products. The results of the simulations show early time arrival of the transmitted wave and discrepancy in the wave velocities. A full optimization of the HVRB model improved the timing of the simulations when compared to the experiments, but still exhibited discrepancies in terms of the velocity. In addition, the new HVRB parameters pushed the CTH synthetic Pop-Plot to be less sensitive the the experimental data. Further analysis into the detonation product EOS and initiation model are needed.

Acknowledgments

We thank H. Anderson for assembling the targets. We thank W. D. Reinhart, T. F. Thornhill, J. R. Martinez, and R. A. Palomino of Sandia's STAR facility for operating the gun and conducting the experiments. We also thank M. L. Hobbs for the use of his recently developed LX-17 SESAME Table and we thank M. R. Baer and R. Schmitt for many useful discussions about this work. Sandia National Laboratories is a multi-program laboratory managed and operated by Sandia Corporation, a wholly owned subsidiary of Lockheed Martin Corporation, for the U.S. Department of Energy's National Nuclear Security Administration under contract DE-AC04-94AL85000.

References

1. Gustavsen, R. L., Sheffield, S. A. and Alcon, R. R., "Measurements of shock initiation in the tri-amino-tri-nitro-benzene based explosive PBX9502: Wave forms from embedded gauges and comparisons of four different material lots," *J. Appl. Phys.*, Vol. 99, p. 114907, 2006.

2. Baer, M. R., Root, S., Dattelbaum, D., Hooks, D. E., Gustavsen, R. L., Orler, B., Pierce, T., Garcia, F., Vandersall, K., DeFisher, S. and Travers, B., "Shockless Compression Studies of HMX-based Explosives," in "Shock Compression of Condensed Matter," Vol. CP1195, p. 699, APS, 2009.

3. Lee, E., Breithaupt, D., McMillan, C., Parker, N., Kury, J., Tarver, C., Quirk, W. and Walton, J., "The Motion of Thin Metal Walls and the Equation of State of Detonation Products," in "8th Symposium (International) on Detonation," p. 613, 1985.

4. Tarver, C. M., Tao, W. C. and Lee, C. G., "Sideways Plate Push Test for Detonating Solid Explosives," *Propellants, Explos., Pyrotech.*, Vol. 21, p. 238, 1996.

5. LaLone, B. M., Fat'yanov, O. V., Asay, J. R. and Gupta, Y. M., "Velocity correction and refractive index changes for [100] lithium fluoride optical windows under shock compress, recompression, and unloading," *J. Appl. Phys.*, Vol. 103, p. 093505, 2008.

6. Dolan, D. H., "Foundations of VISAR Analysis," *Technical Report SAND2006-1950*, Sandia National Laboratories, 2006.

7. Baer, M. R., Root, S., Vandersall, K. V. and Garcia, F., unpublished data.

8. Gustavsen, R. L., Sheffield, S., Alcon, R. R., Forbes, J. W., Tarver, C. M. and Garcia, F.,

"Embedded Electromagnetic Gauge Measurements and Modeling of Shock Initiation in the TATB-Based Explosives LX-17 and PBX 9502," in "Shock Compression of Condensed Matter - 2001," Vol. CP620, p. 1019, APS, 2002.

9. McGlaun, J. M., Thompson, S. L. and Elrick, M. G., "CTH: A Three-Dimensional Shock Wave Physics Code," *Int. J. Impact Eng.*, Vol. 10, p. 351, 1990.

10. Starkenberg, J., "Modeling Detonation Propagation and Failure Using Explosive Initiation Models in a Conventional Hydrocode," in "12^{th} International Detonation Symposium," p. 1001, 2002.

11. Hobbs, M. L., unpublished.

12. Hobbs, M. L., Baer, M. R. and McGee, B. C., "JCZS: An Intermolecular Potential Database for Performing Accurate Detonation and Expansion Calculations," *Prop., Expl. Pryo.*, Vol. 24, p. 269, 1999.

13. Steinberg, D. J., "Equation of State and Strength Properties of Selected Materials," *Technical Report UCRL-MA-106439*, Lawrence Livermore National Laboratory, 1996.

14. Jackson, R. K., Green, L. G., Barlett, R. H., Hofer, W. W., Kramer, P. E., Lee, R. S., Nidick Jr., E. J., Shaw, L. L. and Weingart, R. C., "Initiation and Detonation Characteristics of TATB," in "Sixth Symposium (International) on Detonation," Vol. ONR-ACR-221, p. 755, 1976.

15. Dobratz, B. M. and Crawford, P. C., "LLNL Explosives Handbook: Properties of Chemical Explosives and Explosive Simulants," *Technical Report UCRL-52997*, Lawrence Livermore National Laboratory, 1985.

16. Tarver, C. M., Kury, J. W. and Breithaupt, R. D., "Detonation waves in triaminotrinitrobenzene," *J. Appl. Phys.*, Vol. 82, p. 3771, 1997.

17. Tuttle, L. W., Root, S., Schmitt, R. and Harstad, E., "Requirements for Simulating the Transmitted Wave Profile through Metal Barriers," in "15th International Detonation Symposium," 2014.